Hybrid Control and Protection Scheme for Inverter Dominated Microgrids

Xiaotong Xu[*†], Huiqing Wen[* **], Lin Jiang[†], and Yihua Hu[†]

[*]Department of Electrical and Electronic Engineering, Xi'an Jiaotong-Liverpool University, Suzhou, China
[**]State Key Laboratory of Power Transmission Equipment and System Security and New Technology, Chongqing University, Chongqing, China
[†]Department of Electrical Engineering and Electronics, University of Liverpool, Liverpool, ENG, UK

Abstract

With the high penetration of various sustainable energy sources, the control and protection of Microgrids has become a challenging problem considering the inherent current limitation feature of inverter-based Distributed Generators (DGs) and the bidirectional power flow in Microgrids. In this paper, a hybrid control and protection scheme is proposed, which combines the traditional inverse-time overcurrent protection with the biased differential protection for different feeders with different kinds of loads. It naturally accommodates various control strategies such as *P-Q* control and *V-f* control. The parameter settings of the protection scheme are analyzed and calculated through a fast Fourier transform algorithm, and the stability of the control strategy is discussed by building a small signal model in MATLAB. Different operation modes such as the grid-connected mode, the islanding mode, and the transitions between these two modes are ensured. A Microgrid model is established in PSCAD and the analysis results show that a Microgrid system can be effectively protected against different faults such as the single phase to ground and the three phase faults in both the grid-connected and islanded operation modes.

Key words: microgrid protection, distributed generators, inverse-time overcurrent protection, biased differential protection, grid-connected mode, islanded mode

I. INTRODUCTION

Sustainable energy based Distributed Generators (DGs) such as wind turbines, PV modules, and fuel-cells shows environmental advantages when compared with conventional energy sources such as fossil fuels and have been widely utilized [1]-[3]. With the high penetration of various sustainable energy sources, Microgrids have been proposed to integrate multiple DGs and loads for different operation conditions [4]-[7].

Compared with the simple radial connection of conventional power systems, Microgrids have become complicated due to their multiple-source structure [8-10]. Thus, conventional protection schemes are ineffective in Microgrids because fault current becomes bidirectional and changeable due to the existence of multiple DGs. In traditional power systems, fault current is unidirectional and decreased along the feeder. The short-circuit capacity is enlarged and the current path can even reverse due to the cross-connection of DGs and different faults types. Considering the wide use of inverters, fault current is limited to 2 times of the rated current, which is much lower than fault current with the conventional protection scheme. Microgrids show distinct faults characteristics in the grid-connected mode and in the islanding mode. Furthermore, Microgrids are open to new DGs due to their plug-and-play capability. In addition, the dynamic output characteristics of DGs are unpredictable. All of these factors add to the difficulty in the control and protection of Microgrids.

In the control of Microgrids, the concept of peer-to-peer is used to ensure that no critical components are specified such as a master controller or a central storage unit [11]. In Microgrids, different modes such as grid-connected mode and islanding mode are included. Therefore, different control strategies such as the *P-Q* control and *V-f* control are used [12]. The impact of operation mode transitions on critical loads and DGs is discussed in [13]. However, the conventional methods for distributed power systems show poor flexibility and expansibility in terms of Microgrid control, the worst case being a system collapse.

For the protection of Microgrids, extra devices or components such as Fault Current Limiters (FCLs) are commonly used. For instance, Static Series Compensators (SSCs) are often inserted in the main grid side and overcurrent relays can detect decreased fault current for both the grid-connected mode and islanded mode [14]. Energy storage devices are used to facilitate fault current detection especially in the islanded mode [15]. Considering the coordination problem between the fuse and the recloser in Microgrids, a microprocessor based recloser has been applied [16]. FCLs are connected in series with DGs to restrict the fault current [17,

18]. Furthermore, the effects of different arrangements of SFCLs on different fault scenarios in Microgrids [19] are analyzed. However, additional components are required, which add to the system cost and affect the normal operation of Microgrids.

Another method is to analyze the fault characteristics of fault currents in Microgrids and modify the conventional protection schemes. In [20], the phase faults in lines, adjacent lines and branch lines are analyzed and summarized. The characteristics of the fault currents of DGs controlled by *P-Q* and *V-f* for different modes are analyzed in [21]. In [22], an adaptive over current protection is used for distribution feeders by changing the pickup current of the relays. In [23], a relay with a new computing algorithm is designed to improve the reliability and adaptability of Microgrids. However, these methods are complicated when it comes to practical implementation. In [24, 25], current components are analyzed to separate the fault current with traditional overcurrent protection. However, this method is ineffective for symmetrical faults. A comparison between directional overcurrent protection and distance protection is conducted in [26]. This study indicates that directional overcurrent protection is preferred since the fault current entering and leaving the feeder is easily detected and compared. In [27], a Microgrid system is simulated by using differential relays in either the grid-connected or islanded modes for single phase to ground faults. However, the performance of this method for other kinds of faults has not been discussed.

In this paper, a hybrid control and protection scheme combining the traditional inverse-time overcurrent protection with the biased differential protection is proposed. The conventional inverse-time overcurrent protection is used to protect feeders without DGs, while the biased differential protection is applied to feeders with DGs. Since the biased differential protection depends on measuring the current in two sides of the protected area, it can detect the bidirectional fault current caused by DGs. In addition, the operating parameters of the biased differential protection can be set and modified according to practical situations easily due to the development of the microcomputer protection. Therefore, the application of the biased differential protection to a Microgrid is flexible. Because the biased differential protection is only responsible for faults in the protected area, and it cannot detect faults that occur out this area. Therefore, the parameter settings of the biased differential protection do not need to cooperate with the parameter settings of the other protection schemes that are used to protect adjacent devices in the unprotected area of the biased differential protection. Consequently, a combination of the inverse-time overcurrent protection and the biased differential protection can minimize the changing of the main grid and the total cost when a Microgrid is connected to the main grid. In addition, the Microgrid can be more stable and safer under the proposed scheme.

In order to verify the proposed control strategy and protection scheme, a Microgrid model is established in this paper. The parameter settings of the control strategy and the protection scheme are discussed and calculated by a fast Fourier transform algorithm and a small signal analysis through MATLAB. The Microgrid model is simulated through PSCAD under a single phase to ground fault (most common) and a three phase fault (most serious). From the simulation results, it can be seen that the proposed scheme is able to effectively detect and isolate different kinds of faults in both the grid-connected and islanded operating modes.

II. MICROGRID CONTROL

A typical Microgrid system is shown in Fig.1, which includes two DGs and three loads. The Microgrid can be connected or disconnected from the main grid by changing the state of the PCC (Point of Common Coupling), and the SS (Static Switch) is used to smoothly change the operating mode of the Microgrid. The parameters of the system are presented in Table I.

In this Microgrid system, DG1 is a photovoltaic module, and DG2 is a micro gas turbine. The photovoltaic module is controlled by Maximum Power Point Tracking (MPPT), and the PV is connected in series with a battery. Therefore, the output power of the PV can be stored in the battery, and the output power from the PV can be regarded as constant in this case.

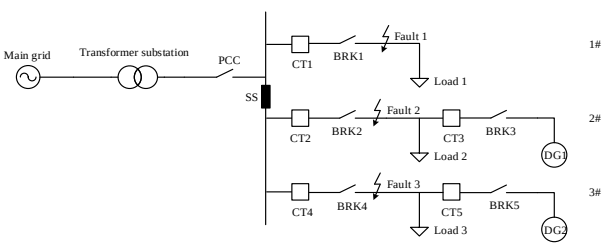

Fig.1. A typical Microgrid system.

A. P-Q and V-f control strategies

In the grid-connected mode, two DGs are controlled by the *P-Q* control method. As a result, the active power and reactive power of the DGs are keep constant for the steady state, and the voltage and frequency of the system are regulated by the main grid. When a fault is detected in the main grid, the operation mode of the Microgrid is changed to the islanded mode. DG2 is still controlled by the *P-Q* method. However, the control method of DG1 is switched to the *V-f* control in order to maintain the stability of the voltage and frequency in the Microgrid, and to keep the balance of the power flow. The detailed control principles of the *P-Q* control and the *V-f* control are illustrated in Fig.2 and Fig.3, respectively.

As shown in Fig.2, the *P-Q* control strategy relies on calculating the current reference and then regulating the current to control the inverters through pulse-width modulation (PWM) signals. Then the current reference is obtained by dividing the reference active power and reactive power (P_{ref},

Q_{ref}) by the actual voltage (u). Compared to the *P-Q* control, the *V-f* control is more complicated because more PI controllers are required in the outer voltage loop and the inner current loop. By making use of these two control methods, the Microgrid can operate healthily in both the grid-connected and islanded modes.

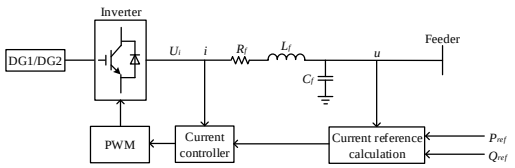

Fig.2. *P-Q* control.

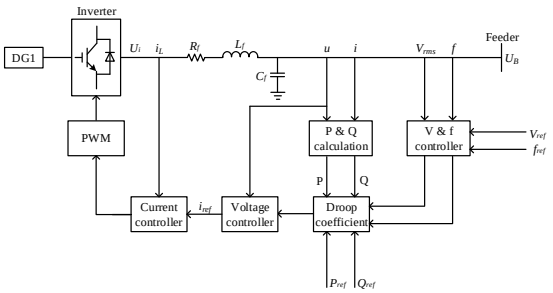

Fig.3. *V-f* control.

B. The stability analysis of the inverter

In order to analyze the stability of the control strategy and to select suitable parameter settings of the PI controller, a small signal model of an inverter is established after converting the data to the d axis and q axis through a Park transform. The control parameter settings of the inverter are shown in Table Ⅱ. Taking the *V-f* control strategy, which is presented in Fig.3, as an example, the state variable Δx is:

$$\Delta x_i = \left[\Delta\varphi_{id}\ \Delta\varphi_{iq}\ \Delta\varphi_{ud}\ \Delta\varphi_{uq}\ \Delta i_{ld}\ \Delta i_{lq}\ \Delta u_d\ \Delta u_q\ \Delta i_d\ \Delta i_q\right]^T \quad (1)$$

where $\dfrac{d\varphi_{id(q)}}{dt} = i_{d(q)ref} - i_{d(q)}$;

$$\frac{d\varphi_{ud(q)}}{dt} = u_{d(q)ref} - u_{d(q)}$$

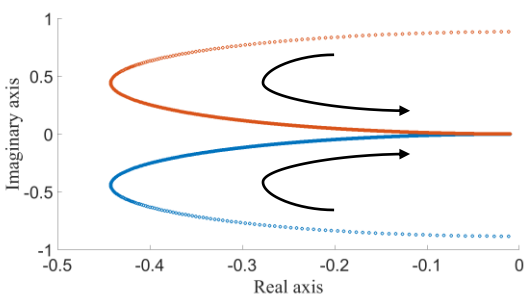

Fig.4. The root locus of an inverter under different proportional gain values.

The input variable Δu is defined as:

$$\Delta u_i = \left[\Delta u_{Bd}\ \Delta u_{Bq}\ \Delta\omega\right]^T \quad (2)$$

The output variable Δy is equal to:

$$\Delta y_i = \left[\Delta i_d\ \Delta i_q\right]^T \quad (3)$$

Therefore, the small signal model of the inverter under the *V-f* control is:

$$\begin{cases} \dot{\Delta x} = A\cdot\Delta x + B\cdot\Delta u \\ \Delta y = C\cdot\Delta x \end{cases} \quad (4)$$

Because the outer voltage control loop is in series with the inner current control loop, the total proportional gain (k_p) can be regarded as the product of k_p in these two control loops, while the total integral time constant (k_i) can be seen as the product of k_i in these two control loops. For the purpose of simplifying the analysis, k_p (or k_i) in the outer voltage loop is equal to that in the inner current control loop.

Based on the data in Table Ⅱ and Table Ⅲ, five pairs of eigenvalues of the state matrix A can be obtained. When k_p varies from 0.01 to 100, and the other control parameters are constant, the most representative root locus of this system is shown in Fig.4. It can be seen that the real part of the eigenvalue decreases until k_p is equal to 1. Then the real part of the eigenvalue increases. Hence, the damping of the system reaches its maximum value when k_p is 1, and the stability of the system is its best at this point.

When k_i changes from 0.0001 to 1, and the other control parameters are invariable, Fig.5 shows the root locus for one pair of eigenvalues. It can be found that the real part of the eigenvalue reduces with an increase in k_i. Therefore, the system

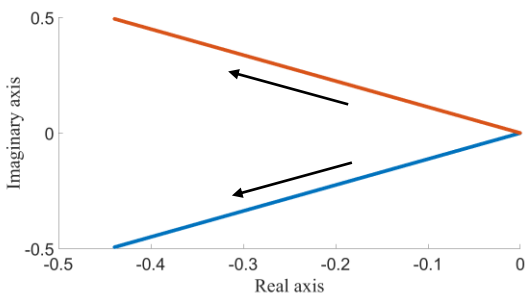

Fig.5. The root locus of an inverter under different integral time constant values.

is stable.

By analyzing the root locus of each eigenvalue, the most suitable values for k_p and k_i are selected. Due to space limitations, the stability and small signal model of the inverter under the *P-Q* control strategy are not discussed in this paper. However, the parameter settings of the PI controller under the *P-Q* strategy can be found in Table Ⅱ.

III. HYBRID PROTECTION SCHEME

In Fig.1, two kinds of loads are considered in the Microgrid

Table I
The parameters of the Microgird

Component	Main grid	Transformer	Load 1	Load 2	Load 3
Data	10kV	25MVA 10kV/0.4kV	0.18MW+ j0.06MVar	0.06MW+ j0.0195MVar	0.06MW+ j0.0195MVar

Table Ⅱ
The control parameter settings of the inverter

Control parameter	V-f control		P-Q control
	Inner current control loop	Outer voltage control loop	Current control loop
Proportional gain	1	1	20
Integral time constant	0.04	0.04	0.001

system: a non-sensitive load in feeder 1 and sensitive loads in feeders 2 and 3. Because the power flow through a feeder without DGs is unidirectional, the inverse-time overcurrent protection is applied to feeder 1 which contains a non-sensitive load [28]. However, for feeder 2 and feeder 3, the inverse-time overcurrent protection cannot be used because the power flows on these two feeders are bi-directional. Therefore, the biased differential protection that relies on measuring the two end electrical variables is used. The principles of these two kinds of protection methods are discussed below.

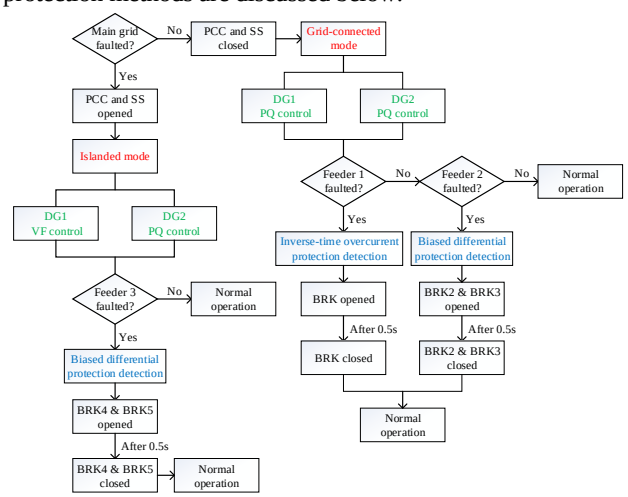

Fig.6. A flow chart of the control and protection.

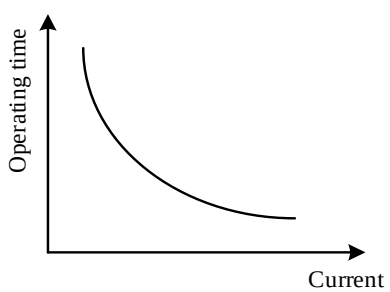

Fig.7. Characteristic of the inverse-time overcurrent protection.

A. Inverse-time overcurrent protection

The inverse-time overcurrent protection is based on measuring the fault current through a relay. When the fault current is bigger than the setting value, the relay operates to trip the related circuit breaker [29]. The tripping time has an inversely proportional relationship with the fault current. For a bigger fault current, the relay operates more quickly [30]. The characteristic of the inverse-time overcurrent protection is illustrated in Fig.7, and time-current equations used in this paper are:

$$t_{trip}(I) = T_D \cdot \left(\frac{A}{M^P - 1} + B \right) + K \tag{5}$$

$$t_{reset}(I) = T_D \cdot \left(\frac{t_r}{1 - M^2} \right) \tag{6}$$

where t_{trip} is the operating time of a tripping; t_{reset} represents the operating time of a resetting; t_r is the reset time when the current is zero; T_D represents the time dial options; M represents the ratio of the actual current to the rated current; and A, B, K and p are the time constant values of the operation characteristic.

B. Biased differential protection

The basic principle of this method is to compare the directional current of two terminals on the line and have the relays send tripping signals to the corresponding circuit breakers for the purpose of protecting electrical equipment. However, in the Microgrids, there are two cases which refer to faults in the feeder or out of the feeder, as illustrated in Fig.8 and Fig.9, respectively. Assume that the current flowing from the bus to the circuit line is positive. Then the current that goes from the circuit line to the bus is seen as negative. Therefore, if a fault happens between bus 1 and bus 2, the total directional current will be the sum of I_1 (positive) and I_2 (positive) as illustrated in Fig.8. However, if the fault is not in the area between bus 1 and bus 2, as shown in Fig.9, the direction of the fault current is opposite (I_1 is positive and I_2 is negative). As a result, the total current in the faulted point is equal to zero, and the differential protection does not operate for this case.

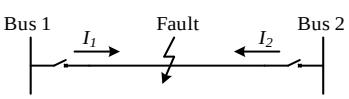

Fig.8. Case One: a fault between two feeders.

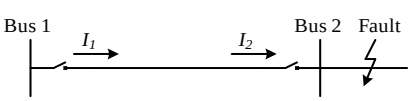

Table III
Initial conditions of the system

Component	Ud (V)	Uq (V)	id (A)	iq (A)	ild (A)	ilq (A)	UBd (A)	UBq (A)	ω(A)
Data	328	0	125	15	125	20	328	0	377

Table Ⅳ
Fault current in the frequency domain

Fault conditions	Grid-connected mode				Islanded mode			
	Single phase to ground fault		Three phase fault		Single phase to ground fault		Three phase fault	
	I_{DG}	I_{grid}	I_{DG}	I_{grid}	I_{DG}	I_{grid}	I_{DG}	I_{grid}
Amplitude (kA)	1.3080	3.2882	0.4824	31.3746	0.2235	1.6280	0.1484	1.0469
Phase (rad)	-1.2967	-1.0189	0.03754	-0.06779	0.6963	0.5941	0.7212	1.3501

Table Ⅴ
Differential and bias current values

Fault conditions	Grid-connected mode		Islanded mode	
	Single phase to ground fault	Three phase fault	Single phase to ground fault	Three phase fault
I_{diff} (kA)	5.1466	31.8570	2.2568	2.3914
I_{bias} (kA)	2.6421	15.9293	1.2322	1.2224

Fig.9. Case Two: a fault outside of two feeders.

Fig.10. Characteristic of the biased differential protection.

Based on the principle of differential protection, the biased differential protection is used for DGs in feeder 2 and 3. Fig.10 shows the characteristic of this strategy. First the differential current and biased current are calculated from the measured data of the current transformers. Once the point (I_{bias}, I_{diff}) is in the trip area, the relay will operate to isolate the fault. The trip and no trip areas are divided by different slopes (K_1 and K_2). The expressions for the differential and bias current are:

$$I_{diff} = |I_1 + I_2| \tag{7}$$

$$I_{bias} = \frac{|I_1| + |I_2|}{2} \tag{8}$$

where I_1 and I_2 are the phasor currents of the secondary current transformer.

The characteristic of the biased differential protection can be expressed as:

$$\text{If } |I_{bias}| < I_{s2},\ |I_{diff}| > K_1 \cdot |I_{bias}| + I_{S1} \tag{9}$$

$$\text{If } |I_{bias}| \geq I_{s2},\ |I_{diff}| > K_2 \cdot |I_{bias}| - (K_1 - K_2) \cdot I_{S2} + I_{S1} \tag{10}$$

where K_1 and K_2 are the settings of the percentage bias, and I_{S1} is the minimum pickup current of the relay.

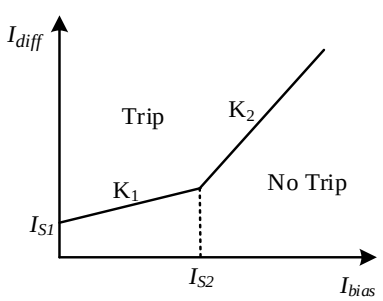

C. Parameter settings for relays

By using the FFT (Fast Fourier Transform) in MATLAB, the simulation result in PSCAD can be transformed from the time domain to the frequency domain. Therefore, the features of fault currents are easily obtained. Then the parameters of the overcurrent and current differential relays can be set after the calculations.

Taking a single phase to ground fault in the grid-connected mode (fault 2) as an example, the amplitude and phase values of the DG1 side fault current which are converted by a FFT algorithm are presented in Fig.11. Making use of (7) and (8), the differential and biased current can be calculated by:

$$|I_{diff}| = |I_{CT2} + I_{CT3}| = |1.3080 - j1.2967 + 3.2882 - j1.0189| = 5.1466kA \tag{11}$$

$$|I_{bias}| = \frac{1}{2} \times (|I_{CT2}| + |I_{CT3}|) = \frac{1}{2} \times (|1.3080 - j1.2967| + |3.2882 - j1.0189|) = 2.6421kA \tag{12}$$

The other fault current values in the frequency domain under different operating modes and fault types are presented in Table Ⅳ. Meanwhile, Table Ⅴ shows all of the calculation results of the differential and bias current. Then these calculation results can be labelled on the characteristic curve of the biased differential protection shown in Fig.12. These faulted points should in the tripping area for the purpose of opening the corresponding circuit breakers to isolate a fault in any fault case.

According to [31], the percentage bias setting of the biased differential protection is 0.3-0.8 in the general case, and it is recommended to keep the percentage bias setting bigger than

0.5. However, the percentage bias setting should rely on the operating data of devices, and malfunctions should be taken into account in real power systems. Therefore, the percentage bias setting depends more on the real operating conditions of the system, and this value is easy to reset by applying the microcomputer protection. There is no principle for the parameter settings of the biased differential protection in the Microgrid. Therefore, in this paper, the percentage bias settings for K_1 and K_2 are set to 0.5 and 1.5 respectively in order to ensure the reliable operation of the circuit breaker for different fault cases. Finally, the operation equations of the biased differential protection are determined by:

$$\text{When } |I_{bias}| < 2kA,\ |I_{diff}| > 0.5 \cdot |I_{bias}| + 0.05 \quad (13)$$

$$\text{When } |I_{bias}| \geq 2kA,\ |I_{diff}| > 1.5 \cdot |I_{bias}| - 1.95 \quad (14)$$

For the inverse-time overcurrent protection, a FFT can also be used for transforming the fault current from the time domain to the frequency domain. Therefore, the pickup current of the overcurrent relay is easy to obtain, and the other fixed parameter settings for the overcurrent relay are shown in Table Ⅵ [32].

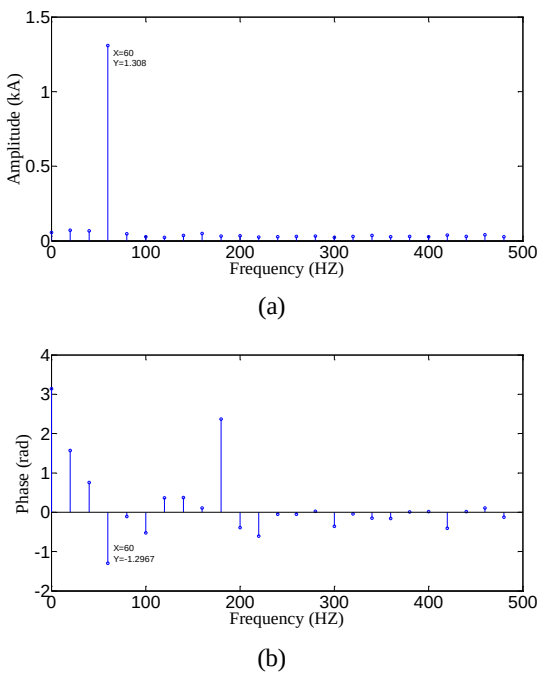

Fig.11. Amplitude and phase values of the DG1 side fault current in the frequency domain under fault 2. (a) The amplitude value. (b) The phase value.

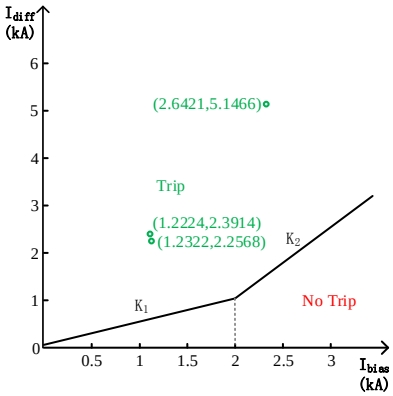

Fig.12. Characteristic curve of the biased differential protection for the simulation model.

IV. SIMULATION ANALYSIS

In this section, different kinds of faults are tested in a Microgrid model to evaluate the validity of the proposed protection scheme. One is a single phase to ground fault, which is the most common type of fault in electrical power systems. The other one is a three phase fault, which represents the most serious type of fault in Microgrids. For each kind of fault, three fault scenarios are defined. Fault 1 and fault 2 are applied to feeder 1 (without a DG) and to feeder 2 (with DG1) independently in the grid-connected mode, while fault 3 occurs on feeder 3 (with DG2) in the islanded mode as shown in Fig.1. Table Ⅵ lists the main parameters of the inverse-time overcurrent protection and the biased differential protection.

The working process of the proposed protection scheme is illustrated in Fig.6. When the Microgrid operates in the grid-connected mode, all three feeders are connected to the main grid. If a fault occurs on feeder 1, it should be detected by the inverse-time overcurrent protection. Then the circuit breaker on feeder 1 (BRK1) should open to isolate the fault after receiving the tripping signal from the relay. The biased differential protection is used to protect feeder 2. Therefore, BRK2 and BRK3 operate if a fault occurs on feeder 2. First, the differential current and biased current are calculated based on the fault current from CT2 and CT3. Second, the relay sends tripping signals to BRK2 and BRK3 if the point (I_{bias}, I_{diff}) is in the trip area. After that, the fault can be isolated from the system by opening BRK2 and BRK3. Because the duration time of every fault is 0.5s, all of the circuit breakers which open in fault conditions reclose again after 0.5s. Then the system can recover to the normal operating condition. The protection process of feeder 3 in the islanded mode is similar to that of feeder 2 in the grid-connected mode. The only difference is that BRK4 and BRK5 are responsible for protecting feeder 3.

A simulation model of a Microgrid and the related protection schemes are established in PSCAD and presented in Fig.13. Four cases are discussed and the main simulation results for different fault scenarios and operating modes are illustrated.

A. Single phase to ground fault in the grid-connected mode

Table Ⅵ
Parameter of the inverse-time overcurrent protection and the biased differential protection

Component	Inverse-time overcurrent protection							Biased differential protection			
	A	B	K	P	tr	q	T_D	I_{S1}	K_1	I_{S2}	K_2
Data	0.0104	0.0226	0	0.02	1.08	2	0.1	0.6	0.2	2	1.5

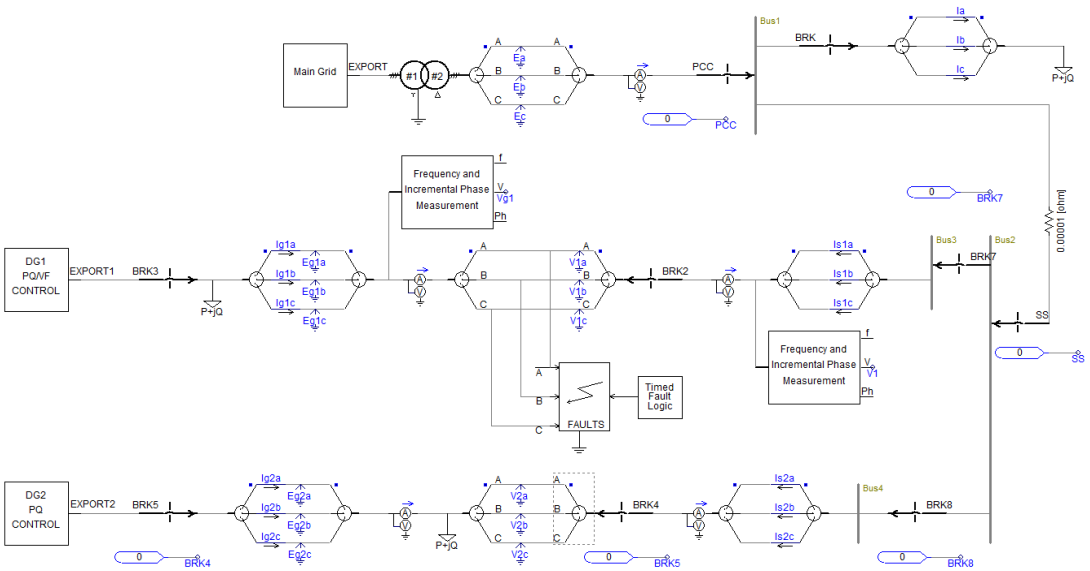

(a)

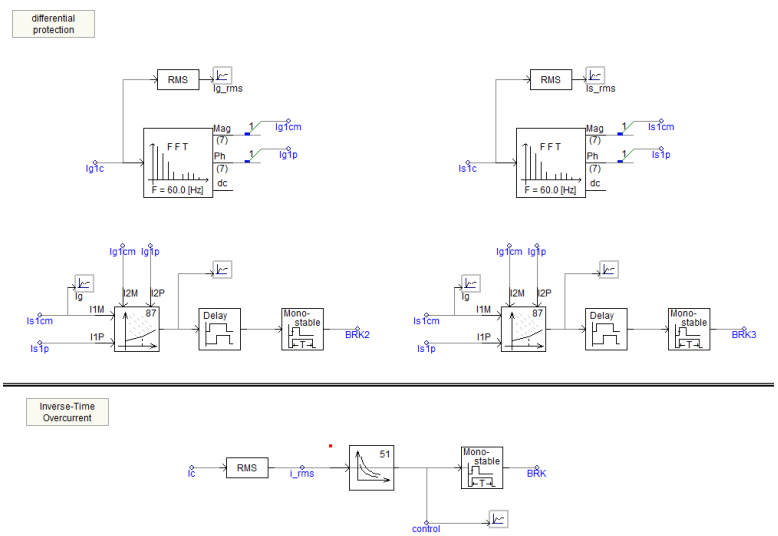

(b)

Fig.13. Simulation model in PSCAD. (a) Microgrid model. (b) Protection model.

In order to check the validity of the protection schemes when the Microgrid operates in the grid-connected mode, phase C to ground faults are applied to feeder 1 and feeder 2. Because there is no sensitive load and the power flow on feeder 1 is unidirectional, the inverse-time overcurrent protection is applied on feeder 1. Fig.14 shows the phase C current of feeder 1. It can be seen that the phase C current suddenly becomes high when the fault occurs at 1.5s, and the fault only lasts for few seconds before it is cleared by BRK1 on feeder 1. The state change of BRK1 can be seen from Fig.15. It changes from 0 to 1 when fault 1 occurs, and BRK1 closes again 2s after the fault is isolated from the system. As a result, the system operates healthily after 2s. Therefore, the inverse-time overcurrent protection scheme is able to detect the fault in feeder 1, and the related circuit breakers can operate to isolate the fault.

The biased differential protection is used to protect the

sensitive load on feeder 2 against fault 2. This protection scheme is based on calculating the values of differential currents and biased currents. These values are obtained from CT2 and CT3 which measure the current in the DG side and the grid side. Simulation curves of the phase C current in the DG1 side and grid side are presented in Fig.16. This figure shows that both the current of phase C in the DG1 side and grid side increases rapidly at 2s when the single phase C to ground fault happens. It also shows that the fault current from the grid side is much larger than that from the DG1 side. In order to ensure the power supply in the other part of the system during the fault, the biased differential protection detects this fault and sends tripping signals to the circuit breakers (BRK2 and BRK3) located on both sides of the fault point. Since fault 2 lasts for a 0.5s duration, BRK2 and BRK3 reclose at 2.5s. Then the current goes back to its normal value.

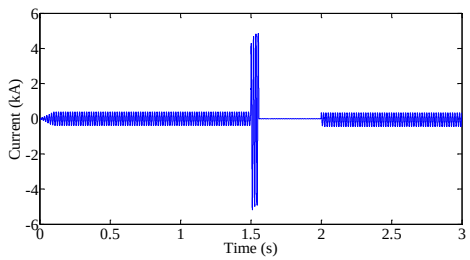

Fig.14. Simulated current of phase C in feeder 1 under a phase C to ground fault (fault 1).

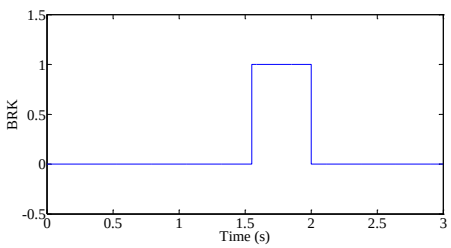

Fig.15. State change of the circuit breaker in feeder 1 under a phase C to ground fault (fault 1).

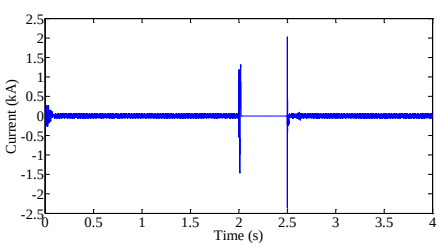

(a)

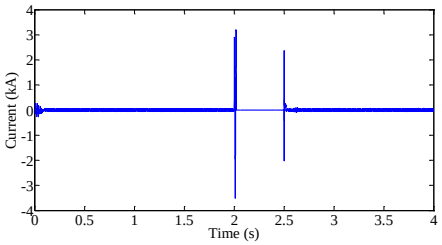

(b)

Fig.16. Simulated current of phase C in feeder 2 under a phase C to ground fault (fault 2). (a) The current in the DG1 side. (b) The current in the grid side.

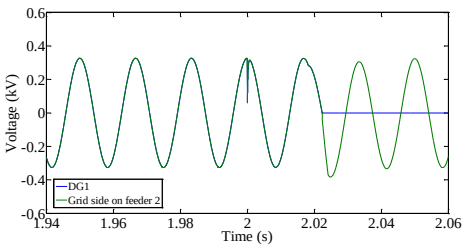

(a)

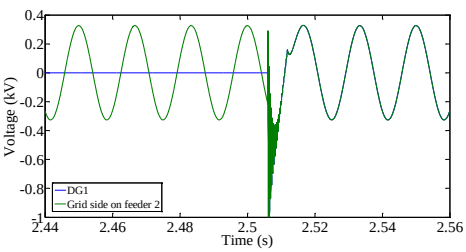

(b)

Fig.17. Simulated voltage of phase C in feeder 2 under a three phase fault (fault 2). (a) Voltage variation during fault 2. (b) Voltage variation after isolating fault 2.

B. Three phase fault in the grid-connected mode

The simulation results of a three phase fault on feeder 1 are similar to those of a phase C to ground fault except for a larger fault current. In addition, the inverse-time overcurrent protection is able to detect and the isolate three phase fault on feeder 1 without a sensitive load. When the three phase fault (fault 2) occurs on feeder 2, the voltage of the DG1 side (the blue line) and grid side (the green line) are shown in Fig.17. The voltages of both the DG1 side and the grid side oscillate when fault 2 occurs at 2s. Then fault 2 is detected by the biased differential protection and related circuit breakers open to clear the fault. Therefore, the voltage of the DG1 side becomes zero, while the voltage of grid side is stable after the oscillation. At about 2.5s, BRK2 and BRK 3 close again, and the voltage of the DG1 side becomes equal to the voltage of the grid side after the synchronization process. Because the DG1 is controlled by the *P*-*Q* method, the active power and reactive power of the

DG1 should remain constant (0.04MW and 0.01MVar) as shown in Fig.18. Therefore, it is concluded that the control strategy and protection scheme are effective in the grid-connected mode.

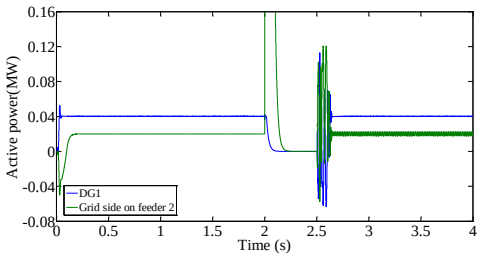

(a)

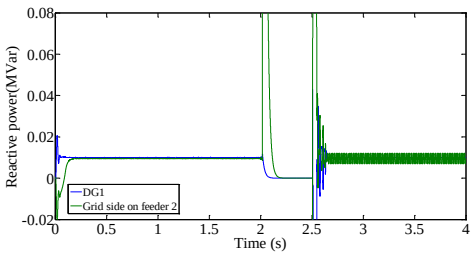

(b)

Fig.18. Simulated active power and reactive power in the DG1 side and grid side under a three phase fault (fault 2). (a) Active power. (b) Reactive power.

C. Single phase to ground fault in the islanded mode

To ensure the power supply of some sensitive loads, the operating mode of a Microgrid changes to the isolated mode if a fault happens in the main grid. On this occasion, the PCC and the SS open, and load 1 is separated from the network. In order to regulate the voltage and frequency of the Microgrid, the control strategy of DG1 changes from the *P-Q* control to the *V-f* control, while DG2 is still regulated by the *P-Q* control method. Because load 2 and load 3 are sensitive loads and the power flow on these two feeders are bidirectional, feeder 2 and feeder 3 are protected by the biased differential protection.

Fig.19 shows the current of phase C in the whole simulation process when a phase C to ground fault (fault 3) occurs on feeder 3. The network operates in the grid-connected mode before the Microgrid is disconnected from the main grid at 1s, and the phase C current becomes stable after the oscillation. Then fault 3 happens at 2s, and the current on both sides of the fault point goes up immediately. Based on calculating the differential and biased current from the DG2 side and the grid side, it can be found that this fault current is in the trip area. Therefore, the relay sends tripping signals to the related circuit breakers. The states of BRK4 and BRK5 change from 0 to 1 at 2s, and the currents of phase C both in the DG2 side and the grid side reduces to 0 at the same time. Therefore, the single phase to ground fault can be separated from the network successfully by applying the biased differential protection. The islanded Microgrid can slowly return to the normal condition after 2.5s.

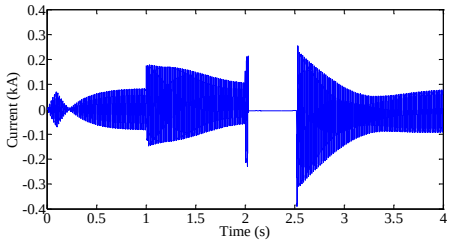

(a)

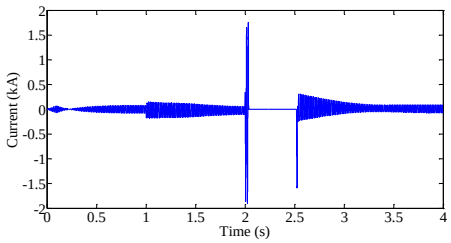

(b)

Fig.19. Phase C current in feeder 3 under a phase C to ground fault (fault 3). (a) Current in the grid side. (b) Current in the DG2 side.

D. Three phase fault in the islanded mode

Compared to the phase C current when a single phase to ground fault occurs on feeder 3, the phase C current is much bigger when a three phase fault occurs on feeder 3. Luckily, the biased differential protection is able to detect this fault and tripping signals are sent to circuit breakers on both the DG2 side (BRK5) and the grid side (BRK4). Therefore, fault 3 can be isolated when the Microgrid operates in the islanded mode regardless of whether the fault type is a single phase to ground or a three phase fault.

Since the Microgrid operates in the islanded mode, it loses the support of the voltage and frequency from the main grid. In this case, the *V-f* control takes the place of the main grid to regulate the voltage and frequency in the Microgrid. Since the stable operation of a Microgrid is very important, load variation cases are added in this part in order to verify the effectiveness of the control strategy. Fig.20 and Fig.21 show detailed simulation results when the system operates in different situations.

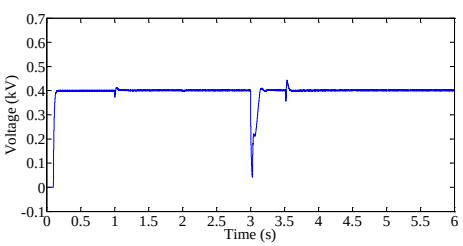

Fig.20. Voltage of a Microgrid in the islanded mode.

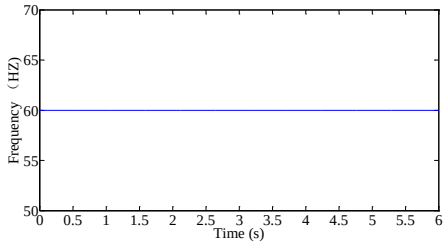

Fig.21. Frequency of a Microgrid in the islanded mode.

Before 1s, the Microgrid operates in the grid-connected mode with a voltage ramp up time of 0.1s, and the total load demand of load 2 and load 3 is 0.12MW+j0.039MVar. The Microgrid is separated from the main grid at 1s, and it operates in the islanded mode. After that, the active power of load 2 increases to 0.08MW at 2s and load 3 remains constant. Because DG2 is controlled by the *P-Q* method and it outputs unchanging power, the output power of DG1 goes up to meet the increased load demand. Meanwhile, the voltage and frequency of the Microgrid system can be kept stable under the *V-f* control applied in DG1. The three phase fault occurs on feeder 3 at 3s. Therefore, the voltage drops a lot and the output power from DG2 becomes zero. Then the fault is cleared by the biased differential protection and the related circuit breakers on feeder 3 close again after 0.5s. The root mean square (RMS) value of the voltage can recover to 0.4kV after the oscillation. At 4.5s, load 3 reduces from 0.06MW+j0.0195MVar to 0.02MW+j0.0005MVar and the output power of DG1 decreases.

In the whole simulation process, the voltage and frequency of the Microgrid can recover to the normal value even under a three phase fault, and the fluctuations of the voltage and frequency are tiny under load variation conditions. DG2 is controlled by the P-Q method. Therefore, the output power from DG2 is constant when the Microgrid operates in the normal case. Therefore, it can be concluded that the proposed control strategy and protection scheme is able to ensure the stability of the Microgrid.

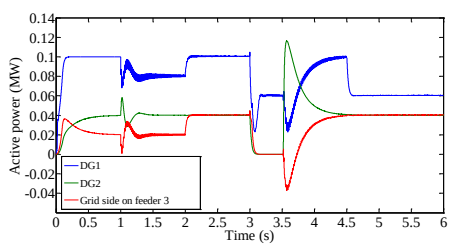

(a)

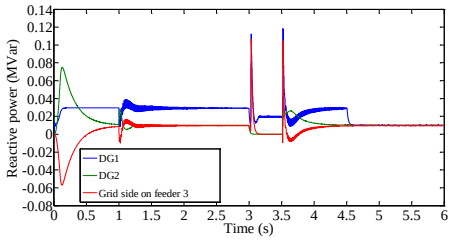

(b)

Fig.22. Active power and reactive power in both the DG2 side and the grid side under a three phase fault (fault 3). (a) The active power. (b) The reactive power.

V. CONCLUSION

This paper focus on simulating and analyzing a hybrid control and protection scheme for a Microgrid. In the proposed control strategy, DGs are regulated by the *P-Q* control and *V-f* control in different operating modes. The inverse-time overcurrent protection and the biased differential protection methods are used for protecting different kinds of loads in the Microgrid model. The feeder with a non-sensitive load is protected by the inverse-time overcurrent protection method, while the feeder with DGs is protected by the biased differential protection method. From the simulation result, it can be seen that this protection scheme is able to protect both kinds of feeders in the grid-connected and islanded modes. In addition, the stability of the Microgrid is high under the proposed control strategy whether the fault type is a single phase to ground fault or a three phase fault.

ACKNOWLEDGEMENTS

This research was supported by the University Research Development Fund (RDF-14-02-03), the State Key Laboratory of Power Transmission Equipment & System Security and New Technology (2007DA10512716414), the Jiangsu Science and Technology Programme (BK20161252), and the National Nature Science Foundation of China (51407145).

REFERENCES

[1] P. Sivakumar and Meenakshi Sundaram Arutchelvi, “Enhanced Controller Topology for Photovoltaic Sourced Grid Connected Inverters under Unbalanced Nonlinear Loading,” *Journal of Power Electronics*, vol. 14, no. 2, pp.369-382 , Feb. 2014

[2] J. Alonso-Mart ńez, J. E. G. Carrasco and S. Arnaltes, “Table-Based Direct Power Control: A Critical Review for Microgrid Applications,” *IEEE Trans. Power Electron.*, vol. 25, no. 12, pp. 2949-2961, Dec. 2010.

[3] Zhongwen Li, Chuanzhi Zang, Peng Zeng, Haibin Yu, Hepeng Li, and Shuhui Li, “Analysis of Multi-Agent-Based Adaptive Droop-Controlled AC Microgrids with PSCAD: Modeling and Simulation,” *Journal of Power Electronics*, vol. 15, no. 2, pp. 455-468, Mar. 2015.

[4] M. Hosseinzadeh and F. R. Salmasi, "Robust Optimal Power Management System for a Hybrid AC/DC

Micro-Grid," *IEEE Trans. Sustain. Energy*, vol. 6, no. 3, pp. 675-687, July 2015.

[5] F. Katiraei, M. R. Iravani and P. W. Lehn, "Micro-grid autonomous operation during and subsequent to islanding process," *IEEE Trans Power Del.*, Vol. 20, No. 1, pp. 248-257, Jan. 2005.

[6] X. Wang, J. M. Guerrero, F. Blaabjerg and Z. Chen, "A Review of Power Electronics Based Microgrids," *Journal of Power Electronics*, vol. 12, no. 1, pp. 181-192, Jan. 2012.

[7] M. R. Miveh, M. F. Rahmat, A. A. Ghadimi, and M. W. Mustafa, "Power Quality Improvement in Autonomous Microgrids Using Multi-functional Voltage Source Inverters: A Comprehensive Review," *Journal of Power Electronics*, Vol. 15, No. 4, pp. 1054-1065, Jul. 2015.

[8] C. Cho, J. H. Jeon, J. Y. Kim, S. Kwon, K. Park and S. Kim, "Active Synchronizing Control of a Microgrid," in *IEEE Trans. Power Electron.*, vol. 26, no. 12, pp. 3707-3719, Dec. 2011.

[9] Z. Zhao, P. Yang, J. M. Guerrero, Z. Xu and T. C. Green, "Multiple-Time-Scales Hierarchical Frequency Stability Control Strategy of Medium-Voltage Isolated Microgrid," *IEEE Trans. Power Electron.*, vol. 31, no. 8, pp. 5974-5991, Aug. 2016.

[10] S. Liu, X. Wang and P. X. Liu, "Impact of Communication Delays on Secondary Frequency Control in an Islanded Microgrid," *IEEE Trans. Ind. Electron.*, vol. 62, no. 4, pp. 2021-2031, April 2015.

[11] J. A. P. Lopes, C. L. Moreira and A. G. Madureira, "Defining control strategies for MicroGrids islanded operation," *IEEE Trans. Power Syst.*, vol. 21, no. 2, pp. 916-924, May 2006.

[12] S. Adhikari and F. Li, "Coordinated V-f and P-Q Control of Solar Photovoltaic Generators With MPPT and Battery Storage in Microgrids," *IEEE Trans. Smart Grid*, vol. 5, no. 3, pp. 1270-1281, May 2014.

[13] A. Micallef, M. Apap, C. Spiteri-Staines and J. M. Guerrero, "Single-Phase Microgrid With Seamless Transition Capabilities Between Modes of Operation," IEEE Trans. Smart Grid, vol. 6, no. 6, pp. 2736-2745, Nov. 2015.

[14] M. Khederzadeh, "Preservation of overcurrent relays coordination in microgrids by application of static series compensators," in *Proc. IEEE DPSP*, 2012, pp. 1-5.

[15] N. Jayawarna and M. Barnes, "Central storage unit response requirement in 'good citizen' Microgrid," in *Proc. EPE*, 2009, pp. 1-10.

[16] S. M. Brahma and A. A. Girgis, "Microprocessor-based reclosing to coordinate fuse and recloser in a system with high penetration of distributed generation," in *IEEE Power Engineering Society Winter Meeting*, 2002, vol. 13, pp. 453–458.

[17] W. El-Khattam and T. S. Sidhu, "Restoration of Directional Overcurrent Relay Coordination in Distributed Generation Systems Utilizing Fault Current Limiter," *IEEE Trans Power Del.*, vol. 23, no. 2, pp. 576-585, Apr. 2008.

[18] W. K. A. Najy, H. H. Zeineldin and W. L. Woon, "Optimal Protection Coordination for Microgrids with Grid-Connected and Islanded Capability," *IEEE Trans. Ind. Electron.*, vol. 60, no. 4, pp. 1668-1677, Apr. 2013.

[19] J. S. Hwang, U. A. Khan, W. J. Shin, J. K. Seong, J. G. Lee, Y. H. Kim and B. W. Lee, "Validity Analysis on the Positioning of Superconducting Fault Current Limiter in Neighboring AC and DC Microgrid," *IEEE Trans. Appl. Supercond.*, vol. 23, no. 3, pp. 5600204-5600204, Jun. 2013.

[20] S. Mirsaeidi, D. Mat Said, M. W. Mustafa and M. Hafiz Habibuddin, "A protection strategy for micro-grids based on positive-sequence component," *IET Renewable Power Generation.*, vol. 9, no. 6, pp. 600-609, Aug. 2015.

[21] E. Casagrande, W. L. Woon, H. H. Zeineldin and D. Svetinovic, "A Differential Sequence Component Protection Scheme for Microgrids With Inverter-Based Distributed Generators," *IEEE Trans. Smart Grid*, vol. 5, no. 1, pp. 29-37, Jan. 2014.

[22] M. Baran and I. El-Markabi, "Adaptive over current protection for distribution feeders with distributed generators," " in *Proc. IEEE PES Power Syst. Conf. Expo.*, Oct. 2004, vol. 2, pp. 715–719.

[23] D. M. Bui, K. Y. Lien, S. L. Chen, Y. C. Lu, C. M. Chan and Y. R. Chang, "Investigate dynamic and transient characteristics of microgrid operation and develop a fast-scalable-adaptable algorithm for fault protection system," *Electric Power Systems Research*, vol. 120, pp. 214-233, Mar. 2015.

[24] R. M. Kamel, M. A. Alsaffar, M. K. Habib, "Novel and simple scheme for Micro-Grid protection by connecting its loads neutral points: A review on Micro-Grid protection techniques," *Renewable and Sustainable Energy Reviews*, vol. 58, pp. 931-942, May. 2016.

[25] S. Mirsaeidi, D. M. Said, M. W. Mustafa, M. H. Habibuddin, K. Ghaffari, "Modeling and simulation of a communication-assisted digital protection scheme for micro-grids," *Renewable and Sustainable Energy Reviews*, vol. 57, pp. 867-878 May. 2016.

[26] F. Coffele, C. Booth and A. Dyśko, "An Adaptive Overcurrent Protection Scheme for Distribution Networks," *IEEE Trans Power Del.*, vol. 30, no. 2, pp. 561-568, April 2015.

[27] M. Dewadasa, A. Ghosh and G. Ledwich, "Protection of microgrids using differential relays," in *Proc. AUPEC*, Australasian, 2011, pp. 1–6.

[28] E. Sortomme, G. J. Mapes, B. A. Foster and S. S. Venkata, "Fault analysis and protection of a microgrid," in *Proc. 40th North Amer. Power Symp. (NAPS'08)*, pp. 1–6.

[29] J. C. Tan, P. G. McLaren, R. P. Jayasinghe and P. L. Wilson, "Software model for inverse time overcurrent relays incorporating IEC and IEEE standard curves," in *Proc. IEEE Canad. Conf. Electrical Computer Engineering*, 2002, pp. 37–41.

[30] C. F. Henville "Combined use of definite and inverse time overcurrent elements assists in transmission line ground relay coordination," *IEEE Trans Power Del.*, vol. 8, no. 3, *pp. 925-932, Jul. 1993.*

[31] X. Li, Z. Zhang, X. Yin, N. Tai and D. Chen, "Selection of settings of differential protection based on fault component," *Power System Techonology*, vol. 25, no. 4, pp.47-50, Apr. 2001.

[32] J. C. Tan, P. G. McLaren, R. P. Jayasinghe and P. L. Wilson, "Software model for inverse time overcurrent relays incorporating IEC and IEEE standard curves," Electrical and Computer Engineering, 2002. IEEE CCECE 2002. Canadian Conference on, 2002, pp. 37-41 vol.1.

Xiaotong Xu was born in Jilin, China. She received her B.S. degree from the Shenyang Institute of Engineering, Shenyang, China, in 2013; and her M.S. degree from the University of Manchester, Manchester ENG, UK, in 2014, both in Electrical Power Systems Engineering. She is presently working towards her Ph.D. degree at the University of Liverpool, Liverpool, ENG, UK. Her current research interests include Microgrid control and protection, and distribution network transformation and optimization.

Huiqing Wen received his B.S. and M.S. degrees in Electrical Engineering from Zhejiang University, Hangzhou, China, in 2002 and 2006, respectively; and his Ph.D. degree in Electrical Engineering from the Chinese Academy of Sciences, Beijing, China, in 2009. From 2009 to 2010, he was an Electrical Engineer working in the Research and Development Center, GE (China) Co., Ltd., Shanghai, China. From 2010 to 2011, he was an Engineer at the China Coal Research Institute, Beijing, China. From 2011 to 2012, he was a Postdoctoral Fellow at the Masdar Institute of Science and Technology, Abu Dhabi, United Arab Emirates. He is presently working as a Lecturer at the Xi'an Jiaotong-Liverpool University, Suzhou, China. His current research interests include bidirectional DC-DC converters, power electronics in flexible AC transmission applications, electrical vehicles, and high-power, three-level electrical driving systems.

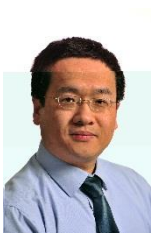

Lin Jiang received his B.S. and M.S. degrees in Electrical Engineering from the Huazhong University of Science and Technology, Wuhan, China, in 1992 and 1996, respectively; and his Ph.D. degree in Electrical Engineering from the University of Liverpool, Liverpool, ENG, UK, in 2001. He is presently working as a Senior Lecturer of Electrical Engineering at the University of Liverpool. His current research interests include the optimization and control of smart grids, electrical machines, power electronics and renewable energy.

Yihua Hu received his B.S. degree in Electrical Motor Drives, and his Ph.D. degree in Power Electronics and Drives, from the China University of Mining and Technology, Jiangsu, China, in 2003 and 2011, respectively. From 2011 to 2013, he was a Postdoctoral Fellow in the College of Electrical Engineering, Zhejiang University, Hangzhou, China. From November 2012 to February 2013, he was an Academic Visiting Scholar in the School of Electrical and Electronic Engineering, Newcastle University, Newcastle upon Tyne, ENG, UK. From 2013 to 2015, he worked as a Research Associate in the Power Electronics and Motor Drive Group, University of Strathclyde, Glasgow, SCT, UK. He is presently working as a Lecturer in the Department of Electrical Engineering and Electronics, University of Liverpool, Liverpool, ENG, UK. He has published more than 36 peer reviewed technical papers in leading journals. His current research interests include PV generation systems, power electronics converters and control, and electrical motor drives.